



ended cylinder was set horizontally at a height of 1 m above the ground, and blast wave pressures were recorded (between  $\theta = 2^\circ$  to  $140^\circ$  at  $\approx 1$  m from the exit) by six pressure gauges and the effect of azimuth angle for the air blast pressure was determined for Pentolite charges of 0.1 kg to 0.5 kg in mass. In addition, numerical simulations were conducted by two-dimensional axisymmetric finite difference code and the results compared with experimental results<sup>9</sup>. Two types of explosive geometries were evaluated in the simulation. One was a cylindrical charge with the same shape as used in the actual experiments and the other was a disk shape charge with a mass equivalent to the cylindrical charge. It was shown that the front of the air blast became convex in the direction of propagation for the cylindrical charge test case. Also, the peak overpressure along this direction was higher in the simulation results than in the actual experimental results. For the disk shape test case, the numerical results of the peak static overpressure agreed very well with the experimental results. However, measurements were conducted at a distance of only 1 m, therefore, decay characteristic of the air blast as a function of distance could not be evaluated. Thus we felt it necessary to obtain blast data at a distance of 2 m and investigate the attenuation index and blast wave characteristics as a function of distance. We also conducted a numerical simulation with a two-dimensional code and compared the simulation results with the experimental results.

## 2. Experiment setup

The explosive used in the experiments was a cast

cylindrical Pentolite charge (PETN:TNT = 50:50 by mass). Tables 1 and 2 show the mass, length, and diameter of the charges. The average density of the charges was  $\approx 1640 \text{ kg} \cdot \text{m}^{-3}$ . A number six electric detonator was used to initiate the explosive charges. Figure 1 shows the experimental setup of the open-ended cylinder with a Pentolite charge of 0.207 kg. Several paper disks ( $\approx 2$  mm in thickness) were used to support the explosive charge. The experiments were conducted at the test site of Asahi Chemical Industry.

Figure 2 shows the test setup including pressure gauges (side and front view). Air blast pressures were measured around the test sample with seven PCB piezoelectric pressure gauges. The pressure gauges were set at azimuth angles of between  $8.2^\circ$  and  $180^\circ$  at intervals of  $\approx 30^\circ$ . Each pressure gauge was flush-mounted to a sharp-edged stainless steel disk (which had a diameter of 90 mm) and mounted in the direction where the peak static overpressure would be measured. The test charge and the pressure gauges were located  $\approx 1$  m above ground so that the reflected blast wave from the ground did not reach the gauge until the primary blast wave at that location had decayed to atmospheric pressure. The open-ended cylinder was welded to a bench and the bench was welded to a steel plate measuring 5 m X 3 m and nominal thickness. Details of the experimental setup and the data collection methods (including initiation methods) are in a previous paper<sup>8</sup>.

## 3. Numerical simulation

The simulation code employed was the

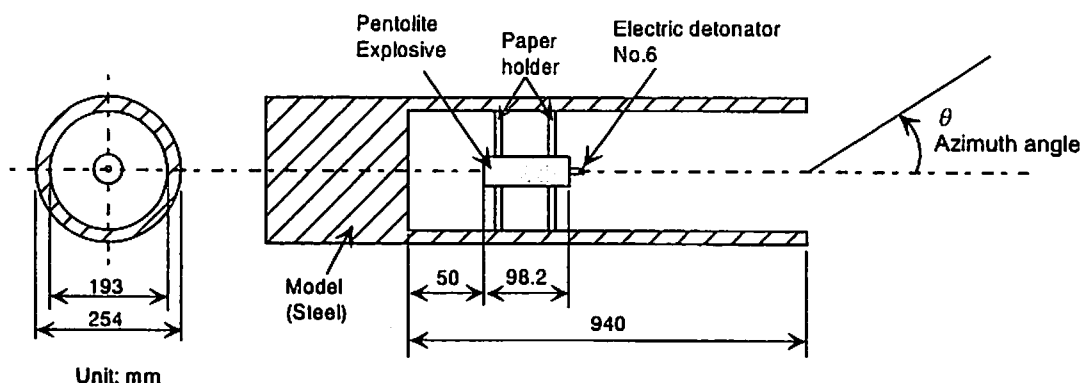


Fig. 1 Schematic cross sectional view of the model cylindrical vessel. The explosive length denotes the case of pentolite 0.207 kg.

Table 1 The observed results of four blast characteristic parameters at 1 m

Charge size*	R(m)	$\theta$ (deg.)	$P_s$ (Pa)	TOA(s)	TOD(s)	$I_s$ (Pa·s)
0.0917 43.6 40.5	0.936	2.0	2.225E5	1.196E-03	0.455E-03	56.19
	1.057	29	1.970E5	1.486E-03	0.554E-03	30.10
	1.022	61	1.287E5	1.689E-03	0.739E-03	30.01
	0.995	87	7.276E4	1.946E-03	0.758E-03	17.88
	1.006	118	2.840E4	2.450E-03	0.995E-03	10.47
	0.992	141	—	—	—	—
0.0916 43.7 40.5	0.981	1.9	3.398E5	1.046E-03	0.633E-03	51.74
	1.089	29	2.168E5	1.513E-03	0.583E-03	31.98
	1.037	60	1.305E5	1.675E-03	0.767E-03	31.04
	0.997	86	7.332E4	1.896E-03	0.663E-03	19.84
	0.991	117	3.383E4	2.354E-03	1.005E-03	11.69
	0.965	141	2.115E4	2.592E-03	1.230E-03	8.585
0.0910 43.2 40.5	0.998	1.8	4.770E5	1.283E-03	0.329E-03	52.57
	1.105	29	2.224E5	1.543E-03	0.581E-03	31.92
	1.047	60	1.387E5	1.684E-03	0.849E-03	31.20
	0.999	85	8.445E4	1.892E-03	0.751E-03	21.24
	0.976	117	3.807E4	2.329E-03	0.921E-03	12.53
	0.945	141	2.215E4	2.605E-03	0.884E-03	9.097
0.195 92.2 40.5	1.013	1.8	7.087E5	1.081E-03	1.047E-03	132.3
	1.105	29	3.816E5	1.291E-03	0.496E-03	39.15
	1.047	59	1.752E5	1.466E-03	0.978E-03	41.83
	0.999	83.9	1.143E5	1.733E-03	0.684E-03	28.78
	0.976	115	4.102E4	2.201E-03	0.667E-03	13.35
	0.945	140	2.246E4	2.478E-03	0.940E-03	10.88
0.487 230.1 40.5	1.051	1.7	1.278E6	0.991E-03	0.381E-03	235.0
	1.151	28	9.925E5	1.146E-03	0.106E-03	67.28
	1.072	58	2.954E5	1.359E-03	0.398E-03	54.12
	1.005	82	1.565E5	1.604E-03	0.765E-03	39.95
	0.959	114	5.332E4	2.032E-03	1.021E-03	22.39
	0.911	139	2.386E4	2.300E-03	1.410E-03	15.98

\*Then values from top to bottom in a cell mean charge mass (kg), length (mm), and diameter (mm), respectively.

AUTODYN-2D Euler code<sup>10)</sup>. The simulation was performed in three stages at different grid resolutions. For the first 200  $\mu$ s the cell size was chosen at  $\approx 4 \text{ mm} \times 4 \text{ mm}$  ( $0 \leq x \leq 940 \text{ mm}$  and  $0 \leq r \leq 96.5 \text{ mm}$ ). Then the simulation was performed using a  $8 \text{ mm} \times 8 \text{ mm}$  grid resolution ( $0 \leq x \leq 2724 \text{ mm}$  and  $0 \leq r \leq 1367 \text{ mm}$ ) up to about 1.2 ms, and finally extended to an  $\approx 16 \text{ mm} \times 16 \text{ mm}$  grid ( $-1195 \leq x \leq 3489$  and  $0 \leq r \leq 2477 \text{ mm}$ ) until the end of the simulation at 10 ms. The origin of the x direction in the

simulation was the end wall of the vessel. The mass and the diameter of the Pentolite charges are shown in the left hand column of Tables 1 and 2. The charges were set 50 mm apart from the end wall of the cylinder. The thermo-equilibrium code CHEETAH<sup>11)</sup> was used to determine the parameters of detonation products for Pentolite when employing a JWL Equation of State (EOS). The EOS for the detonation products was converted into an ideal gas EOS at a volume of more than a hundred times

Table 2 The observed results of four blast characteristic parameters at 2 m

Charge size*	R(m)	$\theta$ (deg.)	$P_s$ (Pa)	TOA(s)	TOD(s)	$I_s$ (Pa·s)	
0.104	1.983	8.2	7.880E4	3.154E-03	1.452E-03	36.32	
	1.993	29	—	3.346E-03	—	—	
	1.975	57	5.431E4	3.672E-03	1.260E-03	25.91	
	49.4	2.045	90	2.684E4	4.498E-03	1.284E-03	13.67
	40.8	2.008	119	1.612E4	5.024E-03	1.202E-03	8.51
	1.992	149	1.152E4	5.536E-03	1.192E-03	6.32	
0.104	1.974	180	1.011E4	5.816E-03	1.199E-03	5.96	
	1.983	8.2	7.077E4	3.178E-03	1.270E-03	35.17	
	1.993	29	7.883E4	3.382E-03	1.531E-03	43.28	
	1.975	57	5.483E4	3.728E-03	1.194E-03	26.14	
	49.5	2.045	90	—	4.550E-03	1.241E-03	—
	40.6	2.008	119	1.676E4	5.092E-03	1.379E-03	8.86
0.207	1.992	149	1.096E4	5.610E-03	1.316E-03	6.45	
	1.974	180	8.277E3	5.898E-03	1.499E-03	5.70	
	1.983	8.2	1.759E5	2.146E-03	2.046E-03	55.17	
	1.993	29	1.414E5	2.800E-03	1.615E-03	78.98	
	1.975	57	9.252E4	3.246E-03	1.442E-03	40.38	
	98.2	2.045	90	3.761E4	4.252E-03	1.281E-03	20.52
40.7	2.008	119	1.974E4	4.920E-03	1.470E-03	12.00	
	1.992	149	1.244E4	5.460E-03	1.420E-03	7.60	
	1.974	180	8.417E3	5.792E-03	1.420E-03	6.64	
	1.983	8.2	3.012E5	2.132E-03	3.592E-04	49.68	
0.516	1.993	29	3.262E5	2.362E-03	1.488E-03	167.2	
	1.975	57	1.592E5	2.846E-03	1.404E-03	67.15	
	243.2	2.045	90	5.771E4	3.950E-03	1.329E-03	30.96
	40.9	2.008	119	2.813E4	4.794E-03	1.537E-03	18.51
	1.992	149	1.239E4	5.352E-03	1.662E-03	11.73	
	1.974	180	1.492E4	5.732E-03	2.752E-03	14.83	

\*Then values from top to bottom in a cell mean charge mass (kg), length (mm), and diameter (mm), respectively.

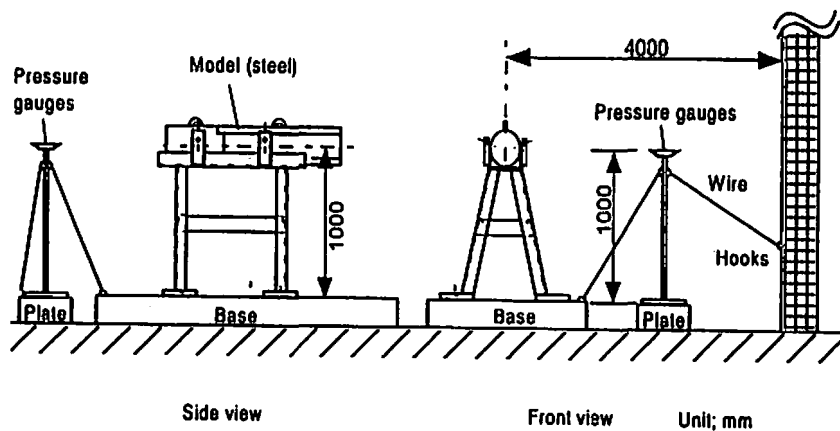


Fig. 2 Setup of the model cylindrical vessel and pressure gauges

that of the initial volume. Air was treated as an ideal gas with a specific heat ratio of 1.4. The open-ended cylinder was treated as a rigid body.

#### 4. Results and discussion

##### 4.1 Pressure contour of air blast waves

It was reported that the finer the mesh size, the stronger the convex shape of the shock front along the direction of propagation. A mesh size of 2 mm × 2 mm resulted in a strong convex shape both inside and outside the vessel as shown in the Fig. 5 of a previous paper<sup>9)</sup>. The reason for this was thought to be due to multiple reflections and focus-

ing between the wall and the central axis of the cylinder. Therefore, in the present simulation, the effects of mesh size on the shape of the shock front were re-examined and a coarser mesh size was used for the first stage of the simulation to avoid a strong convex shape. Figure 3 shows pressure contours at time  $t = 0.5$  ms for charge masses of 0.1 kg, 0.2 kg, and 0.5 kg at a mesh size of 4 mm × 4 mm. It was found that as shock waves discharged from the exit they propagated into a spherical shape for all charge masses. Figure 4 shows the pressure contour at time  $t = 2.2$  ms for a charge mass of 0.1 kg. As the shock wave propagated, the shock front became an almost

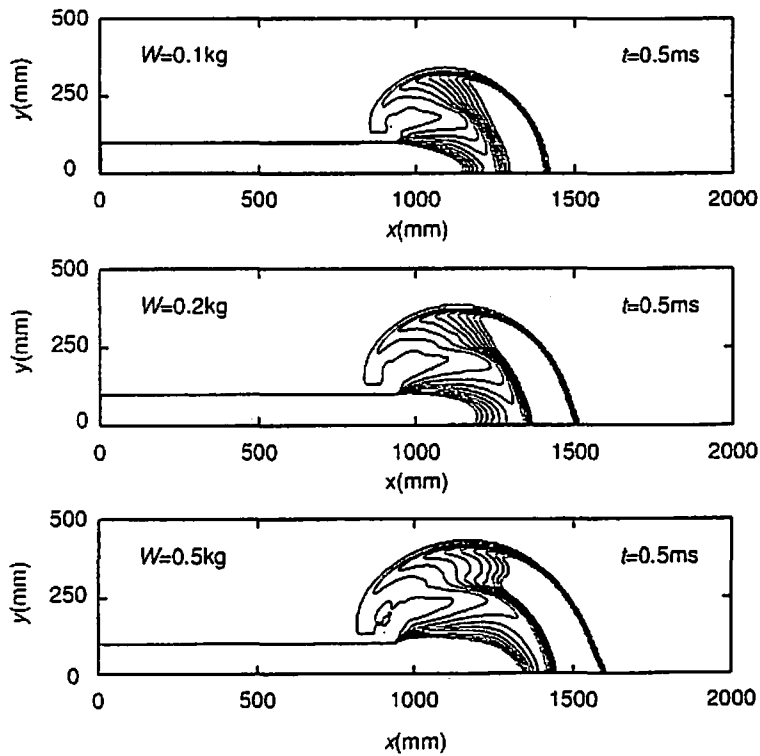


Fig. 3 Simulation result of the pressure contours at time  $t = 0.5$  ms

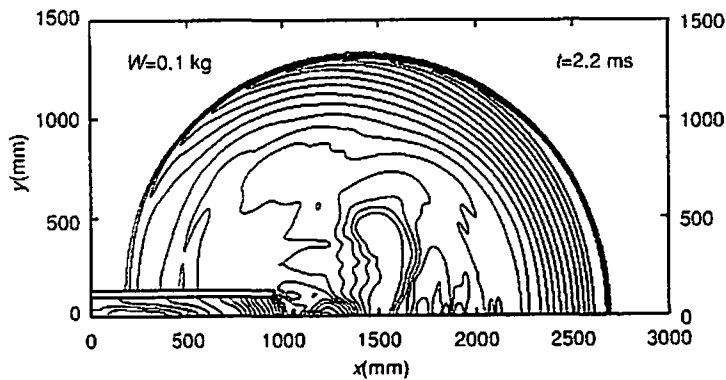


Fig. 4 Simulation result of the pressure contour at time  $t = 2.2$  ms

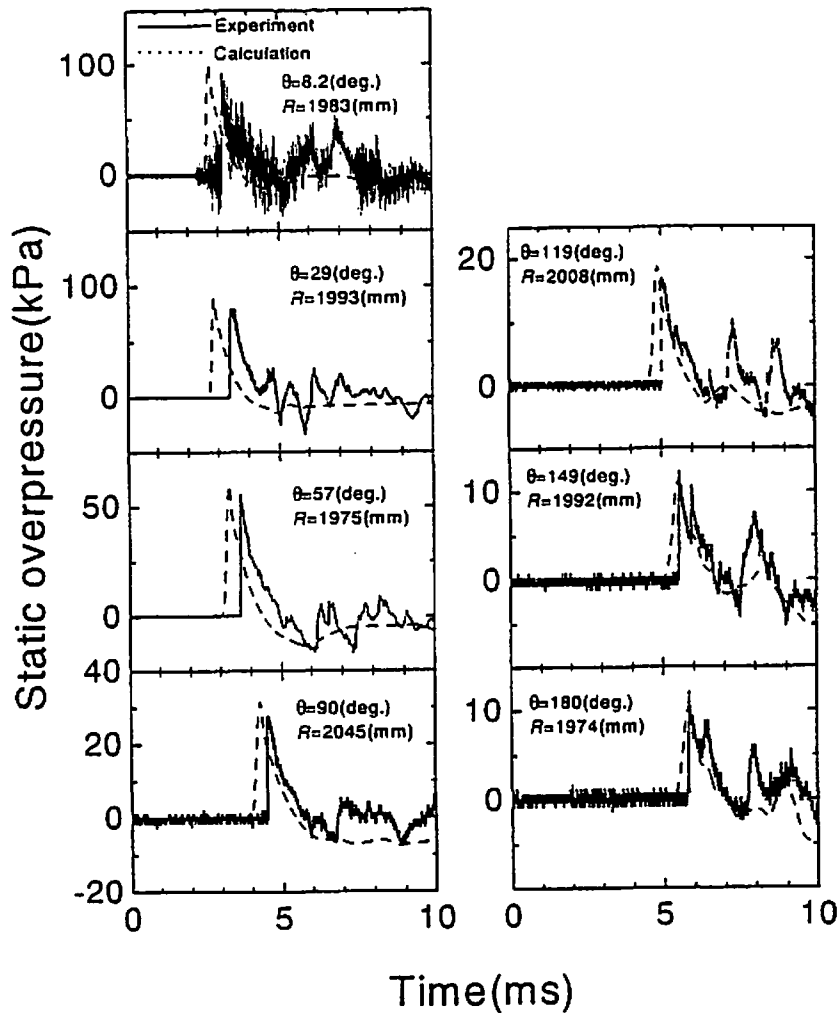


Fig. 5 Pressure-time records of static overpressure for seven azimuth angles. The explosive is a Pentolite 0.104 kg. The solid lines denote the observed data and the broken lines denote the simulation results. The symbols  $\theta$  and  $R$  denote azimuth angle and distance from the exit, respectively.

spherical shape.

#### 4. 2 Static overpressure time records

Figure 5 shows the pressure-time traces at  $\approx 2$  m from the exit (at azimuth angles of  $8.2^\circ$ ,  $29^\circ$ ,  $57^\circ$ ,  $90^\circ$ ,  $119^\circ$ ,  $149^\circ$ , and  $180^\circ$ ) generated by the detonation of a Pentolite charge with a mass of 0.104 kg. The solid lines in Fig. 5 denote the experimental results and the results of the numerical analysis are represented by dotted lines. It was found that the larger the azimuth angle, the lower the peak static overpressure and the slower the time-of-arrival.

Though the fine mesh grid size resulted in higher peak static over pressures in the earlier simulation study, the present simulation results showed a high correlation with the experimental results. Since a

distance error between the center of the explosive and the center of the cylinder was about  $\pm 2$  mm in the experiments, a mesh size of  $4 \text{ mm} \times 4 \text{ mm}$  may yield relatively good agreement in the axisymmetric simulation.

On the other hand, the numerical results showed earlier TOAs than the experiment results. Though a gas effect (dissociation and ionization) for air was not considered in the simulation, this effect should be very weak considering the distance from the charge and therefore not a factor. It is believed rather that the primary reason for this difference is due to a barrier effect caused by the paper holders used for supporting the explosive.

The spikes observed on the experimental waveform were probably caused by reflected shocks from

nearby chamber walls and from the ground. The noisy waveform at an azimuth angle of  $8.2^\circ$  may be caused by the fragmenting paper holders.

#### 4. 3 The decay of peak static overpressure

The time-histories were interpolated by smooth cubic natural spline functions to obtain four characteristic blast parameters: peak static overpressure; time-of-arrival; time-of-duration, and the positive pressure impulse (the time-integral of the overpressure during the positive pressure phase). Tables 1 and 2 show the measured results of these blast parameters at distances of  $\approx 1$  m and 2 m, respectively.

Since insufficient data was available for discussion of this subject in a previous paper, the similarity rule was not discussed in detail. Figure 6 shows the effect of charge mass on peak static overpressure decay with scaled distances for the averaged azimuth angles of  $29^\circ$ ,  $87^\circ$ , and  $144^\circ$ . The open symbol and the closed symbol show the data at the distance of 1 m and 2 m, respectively. The large, medium and small symbols denote the data for 0.5 kg, 0.2 kg, and 0.1 kg, charge masses respectively. It was apparent that a single line could not fit the data for the  $29^\circ$  azimuth angle. This means that a similarity rule is not applicable for the present study. The similarity rule may be valid at larger distances.

Distance attenuation characteristics were investigated from the data obtained at 1 m and 2 m. The empirical formula below (1) was used to evaluate the attenuation of the peak static overpressure as a function of reduced distance.

$$\Delta p = k(R/W^{1/3})^n \quad (1)$$

where  $R$  is distance (in meters) from the exit,  $W$  is the charge mass (in kg),  $\Delta p$  (in Pa) is peak static overpressure,  $k$  is the attenuation constant and  $n$  is the attenuation index. Table 3 shows the values of the charge mass, the azimuth angle,  $k$  and  $n$ . For example, the attenuation index for a charge with a mass of 0.1 kg at azimuth angles of  $\theta = 29^\circ$ ,  $59^\circ$ ,  $87^\circ$ ,  $118^\circ$ , and  $145^\circ$  became  $n = -1.64$ ,  $-1.46$ ,  $-1.55$ ,  $-1.09$ , and  $-0.972$ , respectively. The experimental results by Skjeltop<sup>3)</sup>, Millington<sup>4)</sup>, Nakahara<sup>5)</sup> and Nakayama<sup>7)</sup> are included in Table 3. Skjeltop<sup>3)</sup>

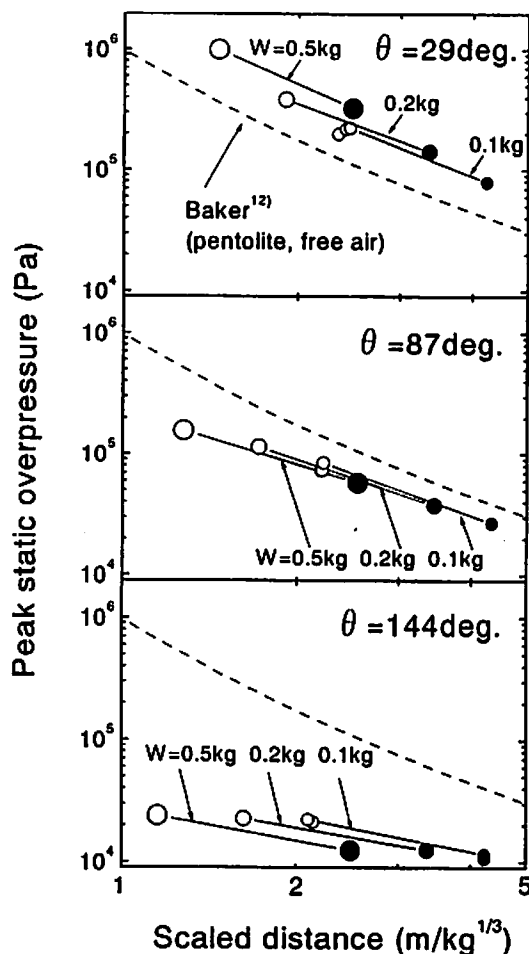


Fig. 6 The decay of peak static overpressure with scaled distance. The open symbols and the closed symbols denote the observed data at about 1 m and 2 m, respectively. The azimuth angles are the averaged values for the three charge masses.

reported that  $n = -1.35$  for azimuth angles of  $0^\circ$  to  $180^\circ$ . However as the azimuth angle increases, the absolute value of the attenuation index decreases for the present study, and decreased to a constant value of  $n = -1$  (which corresponds to the value for a spherically decaying sound wave). Nakayama<sup>7)</sup> reported the same trend. The pressure contours shown in Figs. 3 and 4 also suggest that the shock wave is very weak in the direction of large azimuth angles. It may be reasonable to conclude that attenuation index is a function of azimuth angle.

Also shown in Figure 6 is the standard overpressure for Pentolite in free air which was derived from the data tabulated by Baker<sup>12)</sup> (assuming that heat of explosion of the Pentolite is  $5.1046 \times 10^6 \text{ J} \cdot \text{kg}^{-1}$ , atmospheric pressure is 101.3 kPa, and atmospheric

Table 3 The observed results of the attenuation constant  $k$  and the attenuation index  $n$

Method	Explosive	Charge mass $W$ (kg)	Azimuth angle $\theta$ (deg.)	Constant $k$ (Pa)	Index $n$ (-)	Scaled distance (m/kg <sup>1/3</sup> )
Present	Pentolite (PETN/TNT=50/50 wt.%)	0.096*	29°	8.86E+05	-1.64	2.2-4.2
			59°	4.46E+05	-1.46	
			87°	2.62E+05	-1.55	
			118°	7.93E+04	-1.09	
			145°	4.50E+04	-0.972	
		0.201*	29°	1.17E+06	-1.74	1.7-3.4
			58°	3.24E+05	-1.04	
			87°	2.72E+05	-1.60	
			117°	7.06E+04	-1.04	
			144°	3.34E+04	-0.814	
		0.502*	28°	2.21E+06	-2.10	1.2-2.5
			58°	4.08E+05	-1.05	
			86°	2.23E+05	-1.44	
			116°	6.36E+04	-0.890	
			144°	2.86E+04	-0.910	
Nakayama	TNT	0.2, 0.5, and 1.0	0	5.76E+03	-1.54	5-30
			90	1.57E+03	-1.31	
			180	0.544E+03	-1.16	
Skejeltorp	TNT	0.095-0.152	0, 30, 60, 90, 120, 150 and 180	-	-1.35	1.3-67
Millington	RDX/TNT=60/40wt%	0.163	0, 45, and 90	-	-4/3	1-10
Nakahara	TNT	9.49-343	0	1.67E+06	-1.7	0.7-5

\*The averaged values of the Tables 1 and 2

density is 1.225 kg · m<sup>-3</sup>).

The experimental results of peak static overpressure are higher than that of a free air explosion at small azimuth angles. This observation is very important from a safety standpoint.

#### 4. 4 Comparisons of the experimental results with simulation results

Figures 7, 8, 9, and 10 show the experimental and numerical blast parameters as a function of azimuth angles for charge masses of 0.1, 0.2, and 0.5 kg. The charge characteristics for the Pentolite (charge mass, length and diameter), distances of the pressure gauges, azimuth angles, and the four blast parameters are shown in Tables 1 and 2. The triangular and circular symbols denote the experimental results at 1 m and 2 m, respectively. The solid lines denote the simulation results.

It was found that the larger the azimuth angle, the lower the peak static overpressure. Though the tendency is weaker at greater distances, the pressure at an azimuth angle of 180° is more than one order of magnitude lower than the pressure at ≈ 0°. A good description of this phenomenon is that the strong shock waves propagated forward and the weak pressure waves propagated backward. Since a maximum Prandtl-Meyer function for super sonic expansion flow around a corner is estimated to be 130° for air and the expansion wave can not expand beyond the critical angle, the air blast pressures could be weak larger than the angle. The average measurement error due to the size of the pressure gauges was found to be 3%<sup>8)</sup>. Therefore, from Fig. 7, it is concluded that the experimental peak static overpressures agreed fairly well with the numerical results for all charge masses.

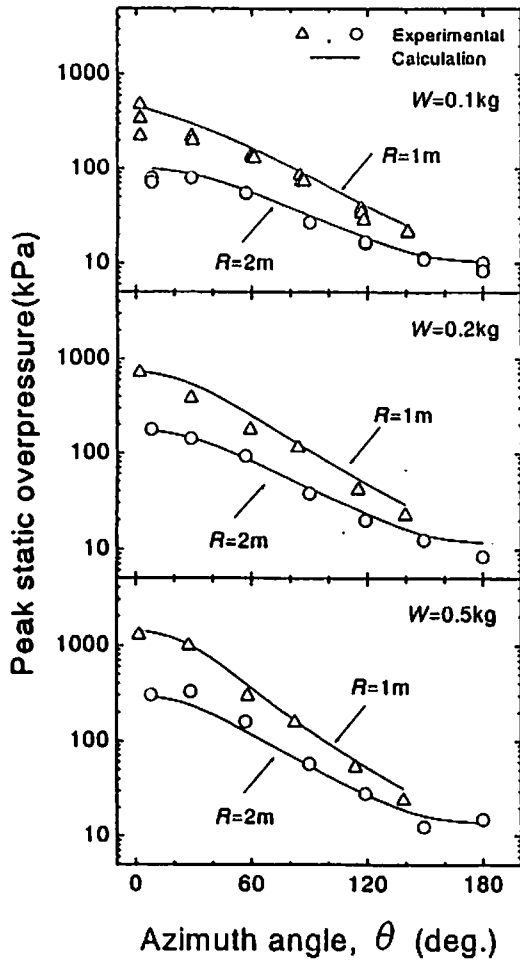


Fig. 7 The peak static overpressure as a function of azimuth angle for the three charge mass at the distances of 1 m and 2 m from the exit

For the TOA, the simulation results showed earlier arrival than the experimental results for all charge masses and at all distances. The systematic deviation of the experimental results from the simulation may be attributed to the effect of the paper disks used for supporting the explosive, as previously mentioned.

For the TOD, since there are some large variations in the experimental results, it may be concluded that the numerical results agreed qualitatively with the experimental results rather than quantitatively.

For the positive impulse, the simulation results were higher than the experimental results, especially at small azimuth angles and at a distance of 1 m. The differences could not be attributable to a measurement error associated with the size of the pressure gauges. The parameters of detonation products for Pentolite were calculated using the

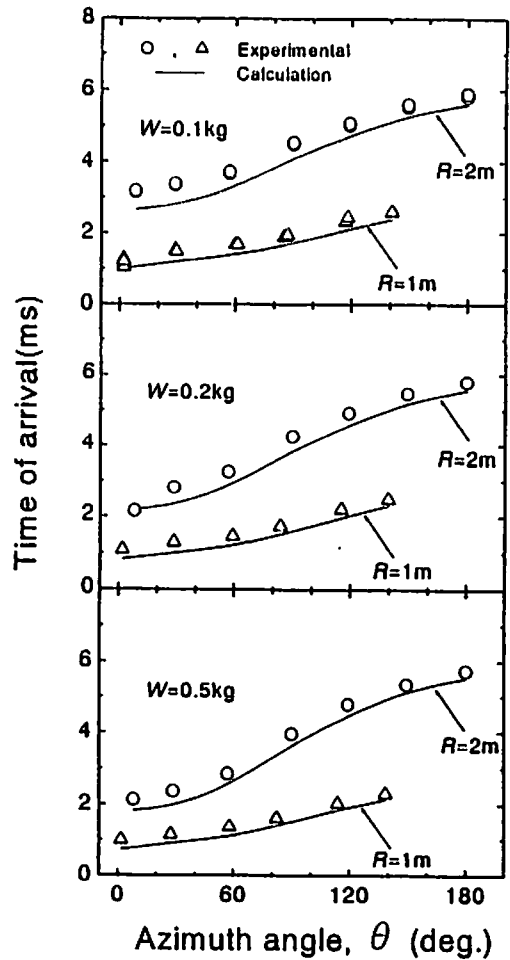


Fig. 8 The time-of-arrival as a function of azimuth angle for the three charge masses at the distances of 1 m and 2 m from the exit

CHEETAH thermo-equilibrium code and employing a JWL EOS. In order to obtain a better agreement between the numerical results with the experimental results, it is necessary to consider the validity of the EOS parameters used in the simulation. For this purpose, the EOS parameters for the Pentolite charge (via cylinder expansion and detonation velocity tests) should be conducted in a future study.

## 5. Conclusions

In order to understand the blast propagation around an open-ended cylinder, blast characteristics were measured by pressure gauges and an AUTODYN-2D numerical simulation was conducted. From an evaluation of the pressure contours, the smaller the mesh size, the stronger the convex shape of the shock front along the center axis and the higher the peak static overpressure. Since the experimental error of the distance between

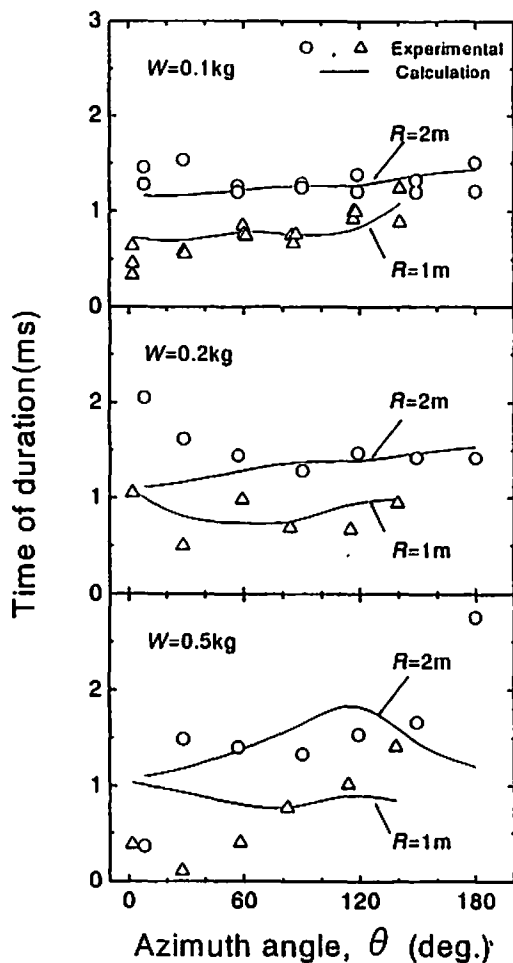


Fig. 9 The time-of-duration as a function of azimuth angle for the three charge masses at the distances of 1 m and 2 m from the exit

the center of the cylinder vessel and that of the explosive was  $\pm 2$  mm, axisymmetric simulation models with a rather coarse mesh size showed better agreement with the experimental results.

From the observed peak static overpressures for the charge masses of 0.1, 0.2, and 0.5 kg, no similarity rule was applicable for the present experiments within measured ranges. The similarity rule may be valid at greater distances. Moreover, when the present results were compared with the data for a free air explosion, it was found that the peak overpressure from the cylinder were higher than that for free air tests at smaller azimuth angles.

The larger the azimuth angle, the weaker the peak static overpressures. In other words, the shock waves propagated forward and the weak pressure waves propagated backward. The directionality of blast wave was weaker at greater distances. It was confirmed, from the experimental and simulation

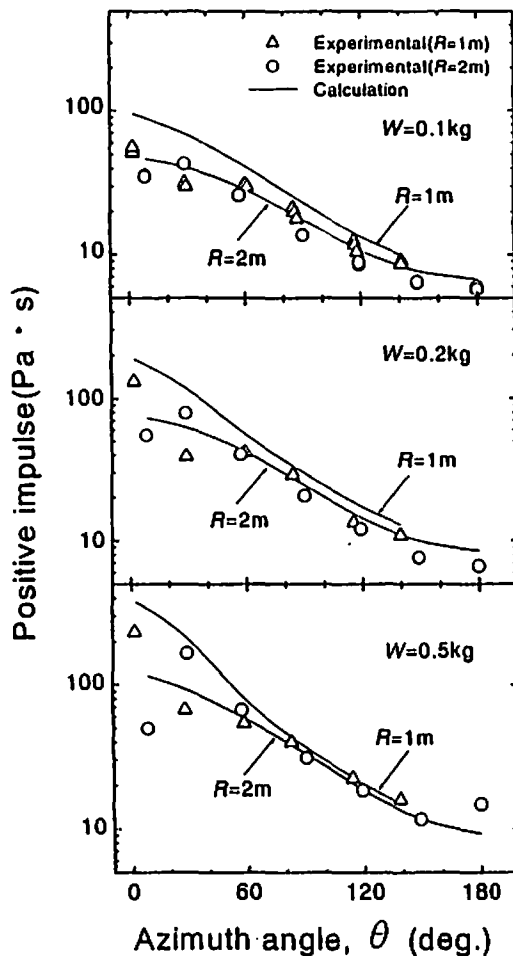


Fig. 10 Positive impulse as a function of azimuth angle for the three charge masses at the distances of 1 m and 2 m from the exit

results, that the attenuation index of peak static overpressures depend on the azimuth angle.

For peak static over pressures, the simulation results agreed reasonably well with the experimental results for all the charge masses. The TOA values generated by the 2D simulation were earlier than the experimental results. The time differences suggested that the paper disks used for supporting the explosive may have retarded the shock waves. A better support method should be used in a future experiments.

Since there were large variations in the experimental TOD, it may be concluded that the numerical results agreed qualitatively with the experimental results rather than quantitatively.

For the positive impulse, the simulation results were higher than the experimental results especially at small azimuth angles and at a distance of 1 m. In order to obtain a better agreement between the

numerical results and the experimental results, it is necessary to measure the EOS parameters and the detonation velocity of the Pentolite charge.

It was demonstrated in this study, that the simulation model is valid for the estimation of the peak static overpressure. From safety stand-points, the present simulation will provide basic data helpful for establishing a safe distance for placement of explosive storage facilities, such as underground magazines.

#### Acknowledgement

The authors would like to thank Dr. M. Haba (Former Special Research Fellow) for his assistance with the simulation modeling.

#### References

- 1) A. T. Skjeltop, T. Hegdahl and A. Jenssen, NDSC Report 81/72, June (1975).
- 2) A. T. Skjeltop, T. Hegdahl and A. Jenssen, NDSC Report 82/72, November (1975).
- 3) A. T. Skjeltop, R. Jenssen and A. Rinnan, Proc. of the Fifth International Symposium on Military Application of Blast Simulators, p. 6:7:1, Stockholm, May (1977).
- 4) C. F. Millington, Minutes of the Twentieth Explosives Safety Seminar, p. 1285 (1982).
- 5) S. Nakahara, A. Motoba, and S. Katoh, Kogyo Kayaku, 46, 219(1985) (in Japanese).
- 6) C. N. Kingery, Technical Report BRL-TR-3012, June (1989).
- 7) Y. Nakayama, T. Matsunaga, M. Iida, and K. Tanaka, Kayaku Gakkaishi, 59, 275(1998) (in Japanese).
- 8) Y. Nakayama, T. Matsumura, K. Miyamoto, M. Iida, and M. Yishida, Kayaku Gakkaishi, 60, 293 (1999) (in Japanese).
- 9) M. Haba, T. Matsumura, Y. Nakayama, and M. Yoshida, Kayaku Gakkaishi, 61, 184(2000) (in Japanese).
- 10) N. J. Robertson, C. J. Hayhurst and G. E. Fairlie, Int. J. of Computer Applications in Technology, 7, 316(1994).
- 11) L. E. Fried, W. M. Howard, P. C. Souers, Cheetah 2.0 User's Manual, Lawrence Livermore National Laboratory, UCRL-MA-117541 Rev. 5 (1998).
- 12) W. E. Baker, "Explosions in Air," (1973), Univ. Texas Press.



## 円筒容器での固体爆薬の爆発による爆風の伝播

中山良男\*, 松村知治\*, 飯田光明\*, 吉田正典\*

一端開放の円筒容器の内部での爆薬による爆風の伝播特性を解明するために、ピエゾ圧力計による計測およびAUTODYN-2Dコードによる計算が行われた。爆風波形は圧力ゲージにより計測され、爆風の4つの特性パラメータが評価され、それらの距離および方位角による減衰特性が検討された。その結果、薬量を0.1, 0.2, 0.5kgと変化させた場合の過剰圧の測定結果より、本実験結果は、爆源に近い距離での計測であったため、爆風の相似則は確認できなかった。また、等圧線の計算結果より、メッシュサイズが小さいと容器正面方向の衝撃波面の形状は突出し、高いピーク静水過圧を与えた。実験では爆薬の設置誤差が±2mm程度存在するため、2次元軸対称の解析結果と比較する場合、4×4mm程度の比較的粗いメッシュによる計算結果が、実験結果を再現することが明らかになった。

空中爆発のデータと比較すると、方位角が小さい領域では、容器内爆発による過剰圧は高くなった。また、容器の正面方向では爆風は強いが、方位角が大きくなると急激に減衰し、音波の特性を有する圧力波となることを見いだした。さらに、距離に対する減衰指数は、方位角に対し一定ではなく、減少することを実験および数値結果より考察した。

過剰圧、到達時間、正圧相持続時間、正圧相インパルスの計算値が実験値と比較された。ピーク静水過圧の計算値は実験値にほぼ一致したが、到達時間の計算値は実験値より速くなった。これは、実験に使用した爆薬保持用の紙製円板の遮蔽効果によると示唆される。持続時間に関しては、実験結果の変動が大きいが、計算結果は実験結果と定性的には一致した。インパルスの計算値は実験値より高めに評価する傾向となった。計算に使用したJWLパラメータの実験的検討が必要である。

(\*独立行政法人産業技術総合研究所 〒305-8565 茨城県つくば市東1-1-1 つくば中央第5)